

Improving Transferable Targeted Attacks with Feature Tuning Mixup

Kaisheng Liang Xuelong Dai Yanjie Li Dong Wang Bin Xiao*

Department of Computing, The Hong Kong Polytechnic University

cskliang@comp.polyu.edu.hk b.xiao@polyu.edu.hk

{xuelong.dai, yanjie.li, dong-comp.wang}@connect.polyu.hk

Abstract

Deep neural networks (DNNs) exhibit vulnerability to adversarial examples that can transfer across different DNN models. A particularly challenging problem is developing transferable targeted attacks that can mislead DNN models into predicting specific target classes. While various methods have been proposed to enhance attack transferability, they often incur substantial computational costs while yielding limited improvements. Recent clean feature mixup methods use random clean features to perturb the feature space but lack optimization for disrupting adversarial examples, overlooking the advantages of attack-specific perturbations. In this paper, we propose Feature Tuning Mixup (FTM), a novel method that enhances targeted attack transferability by combining both random and optimized noises in the feature space. FTM introduces learnable feature perturbations and employs an efficient stochastic update strategy for optimization. These learnable perturbations facilitate the generation of more robust adversarial examples with improved transferability. We further demonstrate that attack performance can be enhanced through an ensemble of multiple FTM-perturbed surrogate models. Extensive experiments on the ImageNet-compatible dataset across various DNN models demonstrate that our method achieves significant improvements over state-of-the-art methods while maintaining low computational cost.¹

1. Introduction

Deep neural networks (DNNs) are highly vulnerable to adversarial attacks [13, 23, 31], raising critical security concerns. In image classification tasks, adversarial attacks can deceive DNNs by adding imperceptible perturbations to benign images, causing the models to produce erroneous predictions. More concerningly, research [9, 10, 46] has demonstrated that adversarial examples possess trans-

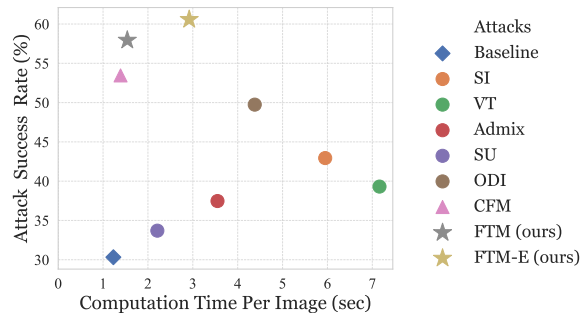


Figure 1. **Effectiveness and efficiency of targeted attacks.** Average attack success rates on 14 black-box models, along with the computation time required to generate an adversarial example. Our methods demonstrate superior performance with low computational cost, surpassing state-of-the-art methods.

ferability properties: adversarial examples generated using one white-box model can successfully fool other black-box models without requiring access to their architectures or parameters. This cross-model transferability of adversarial examples poses severe security threats to real-world AI systems. Therefore, studying the transferability of adversarial examples is crucial for enhancing the robustness of DNNs against such security vulnerabilities.

Targeted transfer-based attacks aim to mislead models into predicting specific target classes, which remains a significant challenge. Due to the lack of knowledge about the target model’s training data and architecture, such attacks tend to generate targeted adversarial examples that overfit to surrogate models and fail to transfer to target models. Various transferable targeted attacks [2, 43, 49] have been proposed but still leave much room for improvement. Notably, data augmentation methods [29, 39, 40] are commonly employed for targeted attacks. But they primarily operate in the image space, while augmentation methods at the feature level remain relatively unexplored. Recently, the Clean Feature Mixup (CFM) method [3] has made important progress by using clean features from random images to disrupt adversarial examples, leading to better targeted

*Corresponding author.

¹Our code is available at <https://github.com/uhiu/feature-tuning-mixup>

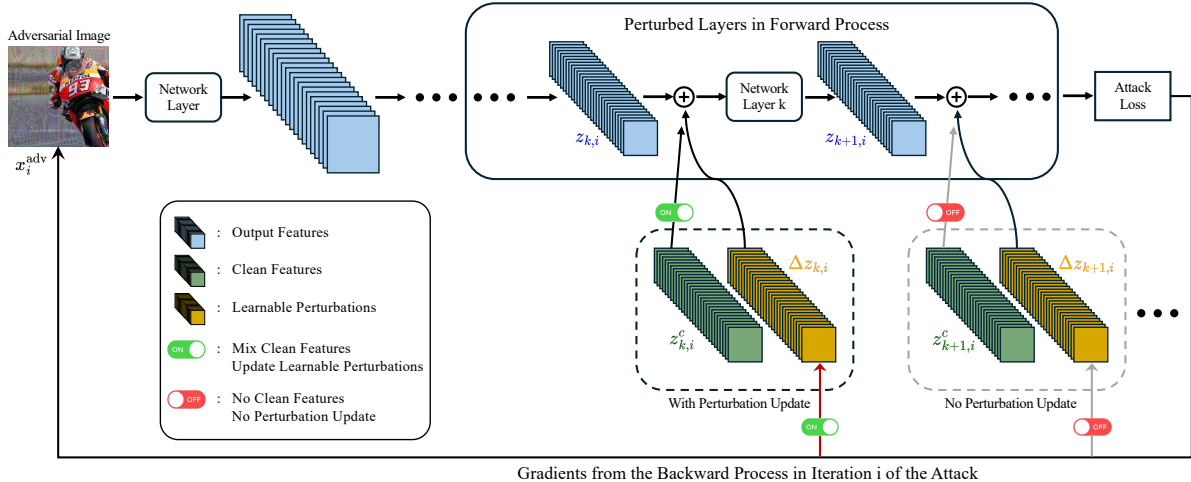


Figure 2. Overview of our FTM attack. In the forward pass, the learnable perturbations are added to the output features. Only a small portion of network layers are randomly selected for perturbation updates and clean feature mixup in each attack iteration. In the backward pass, the gradients of the selected perturbations and adversarial image are computed together for update.

attack success rates (Figure 1). However, CFM uses random clean features without optimizing them specifically for disrupting adversarial examples. We hypothesize that carefully optimized perturbations would be more effective in disrupting adversarial examples, potentially yielding substantial improvements in attack transferability.

In this work, we propose Feature Tuning Mixup (FTM), a novel attack method that optimizes attack-specific feature perturbations to enhance the transferability of targeted adversarial examples. Our method fine-tunes the intermediate features of surrogate models during the attack process by introducing learnable feature perturbations. These feature perturbations are optimized by mixing them with clean features from random images to counteract the adversarial effects of targeted adversarial examples. Through this mechanism, adversarial examples are gradually compelled to become more robust, allowing them to overcome these feature-level disturbances. To address the computational overhead of optimizing feature perturbations, we propose a stochastic update strategy. This strategy initializes the learnable perturbations using values from previous attack iterations and selectively optimizes only a small subset of feature perturbations in each iteration. Ultimately, FTM significantly improves the transferability of targeted adversarial examples while maintaining computational efficiency.

We provide an overview of the proposed FTM in Figure 2. FTM first introduces learnable perturbations into the deep layers of the surrogate model. The learnable perturbations are added element-wise to the original output features before passing to the next layer. In each attack iteration, a small subset of layers is randomly selected and combined with random clean features. Finally, we compute gradients for the learnable perturbations and adversarial im-

age using only one forward and backward pass, similar to standard attacks. We update the selected learnable perturbations and adversarial image, while unselected perturbations remain unchanged. As a result, FTM fully leverages optimized attack-specific feature perturbations, prevents overfitting to surrogate models, and significantly enhances the transferability of targeted attacks.

Our contributions are summarized as follows:

- We revisit feature-level augmentation methods for transferable targeted attacks and identify that incorporating attack-specific feature perturbations, previously overlooked, can efficiently boost existing attacks.
- We introduce Feature Tuning Mixup (FTM), a novel approach that combines random and optimized feature perturbations to enhance targeted transfer-based attacks. Our method includes an efficient stochastic update strategy that maintains computational efficiency while improving attack transferability.
- We conduct extensive experiments across various source and target DNN models on the ImageNet-compatible dataset, demonstrating that our FTM achieves a significant improvement over state-of-the-art methods.

2. Related Work

Adversarial attacks [4, 12, 13, 19, 31] have been widely studied in the field of adversarial learning, including unrestricted attacks [7], physical attacks [26, 27], and black-box attacks [1, 9, 28]. Notably, black-box attacks can be categorized into query-based [1] and transfer-based attacks [9, 28]. The latter, which does not require access to the target DNN model’s outputs, parameters or architecture, is more practical and is the focus of this paper.

2.1. Non-targeted Transfer-based Attacks

Current non-targeted transfer attacks are primarily based on the Iterative-Fast Gradient Sign Method (I-FGSM) [23]. This approach iteratively computes the gradient of the classification loss with respect to the input and updates adversarial examples in the direction that maximizes the loss. However, it often leads to overfitting on white-box models, making the adversarial examples less effective against other black-box models. Numerous studies have explored solutions to the overfitting issue to enhance adversarial transferability. The Momentum Iterative FGSM (MI-FGSM) [9] incorporates a momentum-based optimization method during iterative attacks. Translation-Invariant (TI-FGSM) method [10] enhances the transferability of adversarial examples by achieving translation invariance through gradient smoothing. Data augmentation techniques are widely used to mitigate overfitting. The Diverse Inputs (DI) method [46] employs random resizing and padding with a probability p to generate diverse input, while the Resized Diverse Inputs (RDI) method [50] fixes $p = 1$ and rescales DI-enhanced images back to their original size. The Scale-Invariant (SI) method [29] generates adversarial perturbations using multiple scale transformations, and Admix [40] extends SI by blending images from other labels into the input. Variance Tuning (VT) method [39] randomly selects data points around a given data point and computes their gradients to avoid overfitting. These methods operate in the image space. Feature-level approaches have also been studied to improve adversarial transferability. For instance, the Feature Importance-aware Attack (FIA) [41] identifies and perturbs important features in the intermediate layers of a surrogate model. The Skip Gradient Method (SGM) [44] utilizes more gradients from skip connections. Ensemble-based attacks [9, 30] utilize multiple surrogate models to generate adversarial examples.

2.2. Targeted Transfer-based Attacks

Targeted attacks are more challenging than non-targeted attacks because they not only aim to cause incorrect predictions by the models but also to mislead the models into predicting a specific target class. We can categorize targeted attacks into two types based on whether they require a training dataset. Previous works have utilized training datasets to generate auxiliary modules [21, 22] for transfer-based attacks or directly train a model to generate adversarial examples [32, 42, 47]. This paper primarily focuses on transfer-based attacks that do not require a training dataset.

Targeted transfer-based attacks are widely studied in adversarial machine learning due to their practicality, as they do not require access to the target model’s architecture and parameters, nor do they need training datasets. The Activation Attack (AA) [20] proposes using the distance between adversarial examples and targeted images in feature

space as a loss function, but its attack effectiveness may depend on the selection of targeted images. Po+Trip [24] employs Poincare distance to adapt the gradients’ magnitude and uses triplet loss to address insufficient inter-class distances, but it only works well on target models with similar architectures. Logit Attack (Logit) [49] discovers that a simple logit loss can generate better transferable adversarial examples than CE loss, significantly outperforming previous methods. Self-Universality (SU) method [43] finds that highly universal adversarial perturbations tend to be more transferable for targeted attacks and proposes optimizing the perturbations in different local regions of the image. The Object-based Diverse Input (ODI) method [2] is an efficient data augmentation in image space for targeted attacks using random 3D object and rendering.

Recently, the Clean Feature Mixup (CFM) method [3] proposes a feature-level augmentation which achieves state-of-the-art performance in targeted transfer-based attacks. It stores clean features as random feature perturbations, which mitigates the overfitting to surrogate models. However, the proposed clean features in CFM lack specific optimization for targeted attacks, leaving significant room for improvement. We develop the Feature Tuning Mixup (FTM) method, which effectively and efficiently optimizes attack-specific feature perturbations and significantly improves transferable targeted attacks.

Differences from intermediate-level attacks. This paper investigates feature-level augmentation for targeted attacks, which differs from existing intermediate-level attacks [18, 25, 41, 48]. Our FTM is based on the transfer-based attack framework [23] with logit loss [49], which is currently the most effective framework for targeted transfer-based attacks. In contrast, intermediate-level attacks use loss functions based on a specific intermediate layer, which is hard to apply to targeted attacks. For instance, FIA [41] and NAA [48] require identifying important features based on the true label, while targeted attacks focus on the target label instead of the true label. ILA [18] requires an existing adversarial example as guidance and cannot function as a standalone targeted attack. Therefore, we do not compare FTM with intermediate-level attacks in experiments.

Comparison with adversarial learning methods. Our method learns feature perturbations in an adversarial manner without requiring additional training datasets. While some existing attacks [33, 45] also employ adversarial strategies, they operate in the image space and typically require access to training datasets. For instance, ATTA [45] improves transferability by training an adversarial transformation network to destroy adversarial examples. However, this approach demands substantial computational resources and training data. Like previous work [2, 3, 43, 49], we study targeted transfer attacks without extra data and do not compare with methods that need training data. RAP [33]

utilizes adversarial learning to identify worst-case perturbations in the image space, aiming to locate regions with flat loss landscapes. However, this process requires numerous additional backpropagation steps, leading to prohibitively high computational costs. In contrast, we propose a novel approach that optimizes feature perturbations directly in the multi-layer feature space, an unexplored direction in previous research. Through this innovation, our method achieves superior practicality, effectiveness, and efficiency compared to existing methods.

3. Methodology

3.1. Preliminaries

Problem formulation. For targeted transfer-based attacks, the attacker is assumed to have a white-box surrogate model F , which is a pre-trained image classifier in this paper. We assume that the attacker has no additional training dataset. Given a benign image x , a surrogate model F and a target label y_t , which is different from the true label y of x . The goal of the attack is to generate an adversarial example x^{adv} that is misclassified as y_t by F . The difference between x and x^{adv} should be subtle, and following previous work, we use the ℓ_∞ -norm constraint. The optimization objective can be formulated as:

$$\arg \min_{x^{\text{adv}}} \mathcal{L}(F(x^{\text{adv}}), y_t), \quad s.t. \quad \|x - x^{\text{adv}}\|_\infty \leq \epsilon, \quad (1)$$

where \mathcal{L} is the adversarial loss, e.g., the cross-entropy loss or logit-based loss, and ϵ is the perturbation budget.

MI-FGSM. To solve the problem above, existing methods usually adopt the iterative gradient-based technique, e.g., the MI-FGSM [9], formulated as follows:

$$g_{i+1} = \nabla_x \mathcal{L}(F(x_i^{\text{adv}}), y_t), \quad (2)$$

$$\tilde{g}_{i+1} = \mu \cdot g_i + g_{i+1} / \|g_{i+1}\|_1, \quad (3)$$

$$x_{i+1}^{\text{adv}} = x_i^{\text{adv}} - \eta \cdot \text{sign}(\tilde{g}_{i+1}), \quad (4)$$

$$x_{i+1}^{\text{adv}} = \text{Clip}_{x, \epsilon}(x_{i+1}^{\text{adv}}), \quad (5)$$

where g_i is the gradient of the loss function with respect to the input image x in the i -th iteration. μ is the momentum decay factor, and η is the step size. x_{i+1}^{adv} is clipped within ϵ bound. Initially, we set $x_0^{\text{adv}} = x$ and $g_0 = 0$.

CFM. To improve the transferability of targeted attacks, the Clean Feature Mixup (CFM) method [3] leverages stored clean features to augment adversarial examples, achieving state-of-the-art performance among existing targeted transfer-based attacks. Specifically, it selects outputs from certain network layers as perturbation targets and uses output features from different benign images as feature perturbations. To integrate with MI-FGSM, the feature augmentation in CFM can be formulated as follows:

$$z'_{k,i} = (1 - \alpha_{k,i}) \odot z_{k,i} + \alpha_{k,i} \odot z_{k,i}^c, \quad (6)$$

where \odot denotes element-wise multiplication, $z_{k,i}$ is the input feature to the k -th layer in the i -th attack iteration of MI-FGSM, $z_{k,i}^c$ is a random stored clean feature, and $\alpha_{k,i}$ is a vector representing channel-wise mixing ratios. The network layer k is randomly selected from pre-defined candidate layers with probability p .

3.2. Analysis of CFM

CFM is a powerful *feature-level augmentation* method for targeted attacks. To understand the effectiveness of CFM, we formulate a generalized optimization step for MI-FGSM based on feature-level augmentation as follows:

$$g'_{i+1} = \nabla_x \mathcal{L}(F(x_i^{\text{adv}}; \Delta z_i), y_t), \quad (7)$$

$$\Delta z_i = \{\Delta z_{k,i}, k = 1, \dots, n\}, \quad (8)$$

where $F(x_i^{\text{adv}}; \Delta z_i)$ denotes the surrogate model F with the perturbation Δz_i added to the network outputs in the i -th attack iteration. Equation (7) improves upon Equation (2) by incorporating feature-level perturbations, which is the key idea of CFM. Notably, the perturbation Δz_i represents the collection of perturbations for *all* network layers. We use $\Delta z_{k,i}$ to denote the perturbation for the input of the k -th layer, where n is the maximum layer index of F . Initially, we set $\Delta z_i = 0$. For any layer d that does not require perturbation, we simply set $\Delta z_{d,i} \equiv 0$.

CFM uses clean features to construct Δz_i , and it claims that the rationale is that clean features can suppress the adversarial effect of x_i^{adv} [3]. We formulate this idea in the following equation:

$$\mathcal{L}(F(x_i^{\text{adv}}; \Delta z_i), y_t) > \mathcal{L}(F(x_i^{\text{adv}}), y_t), \quad (9)$$

where Δz_i is supposed to appropriately disrupt adversarial loss in Equation (1) for obtaining robust x^{adv} .

However, clean features are attack-agnostic in nature, as they are not explicitly optimized for the objective in Equation (9). Although CFM demonstrates promising improvements, we argue that there remains unexplored potential in feature-level augmentation for targeted attacks. We believe that integrating attack-specific optimization with attack-agnostic clean features can create a more powerful feature-level augmentation strategy.

3.3. Feature Tuning Mixup (FTM)

We propose Feature Tuning Mixup (FTM), a novel method that uses attack-specific feature perturbations to enhance feature-level augmentation methods. We formulate the optimization problem for learning our feature perturbations and adversarial examples in each attack iteration as follows:

$$\min_{x_i^{\text{adv}}} \max_{\Delta z_i} \mathcal{L}(F(x_i^{\text{adv}}; \Delta z_i), y_t). \quad (10)$$

However, the optimization problem above is challenging to solve from two perspectives: effectiveness and efficiency.

Regarding efficiency, traditional adversarial training [31] often requires multiple steps to optimize Δz_i in each attack iteration, resulting in substantial additional computational cost. As for effectiveness, since Δz_i involves a joint problem across multiple iterations and network layers, inappropriate perturbations can damage the attack effect, which will be shown in our experiments.

Momentum-based stochastic update. We propose a novel technique, momentum-based stochastic update, to optimize Δz_i . We employ one-step optimization with using perturbations in previous iterations as momentum, i.e., Δz_i will be initialized as Δz_{i-1} in Equation (10). Momentum can effectively improve the optimization effectiveness without increasing additional optimization steps. In addition, as we only require one-step optimization, the gradient for Δz_i can be jointly computed with the gradient for x_i^{adv} , which can further speed up the optimization process. To further improve the optimization efficiency, we use a stochastic update strategy, where only the randomly selected layers are updated in each attack iteration. For each selected layer k , it has probability p to be updated in the i -th attack iteration, otherwise, we set $\Delta z_{k,i} = \Delta z_{k,i-1}$. We illustrate the detailed optimization process for FTM in the following.

The forward process for FTM in the i -th attack iteration is formulated as follows:

$$\bar{z}_{k,i} = z_{k,i} + \beta \|z_{k,i}\| \cdot \frac{\Delta z_{k,i}}{\|\Delta z_{k,i}\| + \bar{\epsilon}}, \quad (11)$$

$$z'_{k,i} = \begin{cases} (1 - \alpha_{k,i}) \odot \bar{z}_{k,i} + \alpha_{k,i} \odot z_{k,i}^c, & \tau_k < p, \\ \bar{z}_{k,i}, & \text{else,} \end{cases} \quad (12)$$

where $\beta \|z_{k,i}\|$ is the custom perturbation budget for our feature perturbation $\Delta z_{k,i}$. β is a scaling factor, and $\bar{\epsilon}$ is a small constant. We mix the output feature $z_{k,i}$ and our attack-specific perturbation $\Delta z_{k,i}$ to obtain $\bar{z}_{k,i}$. Then, we use clean features to augment $\bar{z}_{k,i}$ to get $z'_{k,i}$, which is the final perturbed feature that will be fed into the k -th network layer. These perturbed features are computed layer by layer during the forward process. $z_{k,i}^c$ is a random clean feature, and $\alpha_{k,i}$ is a vector representing channel-wise mixing ratio. We randomly sample $\alpha_{k,i}$ from $\mathcal{U}(0, \alpha_{max})$. In each iteration, we randomly sample τ_k from $\mathcal{U}(0, 1)$ to determine whether to update the k -th perturbation $\Delta z_{k,i}$ during the i -th attack iteration. p is the probability threshold.

The backward process for FTM in the i -th attack iteration is formulated as follows:

$$\Delta z'_i = \{(\Delta z_{k,i}, \tau_k) \mid k = 1, \dots, n\}, \quad (13)$$

$$g'_{i+1}, g^{\Delta z'} = \nabla_{x_i^{\text{adv}}, \Delta z'_i} \mathcal{L}(F(x_i^{\text{adv}}; \Delta z'_i), y_t), \quad (14)$$

$$\Delta z_{k,i+1} = \begin{cases} \Delta z_{k,i} + g_k^{\Delta z'}, & \tau_k < p, \\ \Delta z_{k,i}, & \text{otherwise,} \end{cases} \quad (15)$$

Algorithm 1 Feature Tuning Mixup (FTM) Algorithm

Input: Surrogate model F , clean image x , target label y_t , iteration number T , perturbation budget ϵ , input transformation $\phi(\cdot)$ (RDI, etc.), step size η , decay factor μ

Input: Mixing range α_{max} , probability p , mixing ratio β

Output: An adversarial example x^{adv}

- 1: $x_0^{\text{adv}} = x, g_0 = 0$.
 - 2: Initialize perturbation $\Delta z_0 = 0$
 - 3: **for** $i = 0 \rightarrow T - 1$ **do**:
 - 4: Extend $F(x_i^{\text{adv}})$ to $F(\phi(x_i^{\text{adv}}))$
 - 5: Select layers to update and obtain $\Delta z'_i$ from Δz_i
 - 6: Forward and backward pass to get g'_{i+1} and $g^{\Delta z'}$ using Equations (12) and (14)
 - 7: Obtain Δz_{i+1} using Equation (15)
 - 8: Calculate $\tilde{g}_{i+1} = \mu \cdot g_i + g'_{i+1} / \|g'_{i+1}\|_1$
 - 9: Update example $x_{i+1}^{\text{adv}} = x_i^{\text{adv}} - \eta \cdot \text{sign}(\tilde{g}_{i+1})$
 - 10: Clip x_{i+1}^{adv} to be ℓ_∞ -bounded by ϵ
 - 11: **end for**
 - 12: $x^{\text{adv}} = x_T^{\text{adv}}$
 - 13: **return** x^{adv}
-

where $\Delta z'_i$ represents a set containing both perturbations $\Delta z_{k,i}$ and their corresponding random variables τ_k from the forward process, which determines whether each perturbation needs to be updated. $g_k^{\Delta z'}$ denotes the gradient with respect to the k -th perturbation $\Delta z_{k,i}$. The threshold p remains consistent with that used in the forward process. We summarize our FTM attack in Algorithm 1.

Efficiency analysis. FTM does not require complex operations or additional forward and backward passes. Therefore, FTM is theoretically efficient on both CNNs and ViTs. In contrast, SI, VT, Admix, and SU require additional forward and backward passes, while ODI requires a computationally expensive input transformation.

Ensemble of surrogate variants (FTM-E). Observing that FTM can efficiently perturb the surrogate model, we propose to further enhance the attack effectiveness through an ensemble strategy. We create multiple copies of the surrogate model and independently apply FTM to each copy, then ensemble them as a new surrogate model. We empirically show that utilizing an ensemble of two perturbed surrogate models can substantially enhance the attack performance while maintaining reasonable computational costs.

4. Experiments

4.1. Experimental Settings

Datasets. Following prior research [2, 3, 43, 49], we conduct experiments on the ImageNet-compatible dataset from the NIPS 2017 adversarial attack challenge. This dataset comprises 1,000 images, each annotated with both true and target class labels for targeted attack evaluation.

Source	Attack	Time (s)	VGG-16	RN-18	RN-50	DN-121	Xcep	MB-v2	EF-B0	IR-v2	Inc-v3	Inc-v4	Avg.
RN-50	DI	1.37	63.2	56.4	98.9	74.7	5.5	27.8	29.0	5.6	9.0	9.4	37.9
	RDI	1.23	66.3	70.7	98.2	81.9	13.2	46.4	47.2	17.1	29.9	23.3	49.4
	RDI-SI	5.95	70.5	79.8	<u>98.8</u>	88.9	29.5	56.2	66.2	37.9	56.4	43.6	62.8
	RDI-VT	7.16	68.8	78.7	98.2	82.5	27.9	54.5	56.1	32.8	45.8	37.9	58.3
	RDI-Admix	3.55	74.2	80.7	98.7	86.8	20.9	59.4	56.1	26.7	42.7	34.1	58.0
	RDI-SU	2.21	67.9	74.7	98.3	83.3	24.9	56.3	50.2	20.9	32.1	26.2	53.5
	ODI	4.38	78.3	77.1	97.6	87.0	43.8	67.3	70.0	49.5	65.9	55.4	69.2
	RDI-CFM	1.39	84.7	<u>88.4</u>	98.4	<u>90.3</u>	51.1	81.5	78.8	48.0	65.5	59.3	74.6
	RDI-FTM	1.54	<u>86.3</u>	87.5	97.9	89.7	<u>56.1</u>	83.3	81.2	<u>54.7</u>	70.8	<u>66.6</u>	<u>77.4</u>
	RDI-FTM-E	2.92	88.1	88.6	98.3	91.4	59.4	85.4	84.3	56.9	73.4	69.3	79.5
Inc-v3	DI	2.01	2.9	2.4	3.4	5.0	1.9	1.8	3.7	3.0	99.2	4.2	12.8
	RDI	1.76	3.5	3.8	4.0	7.0	3.1	3.0	5.9	6.3	98.7	7.1	14.2
	RDI-SI	8.11	4.0	5.2	5.7	11.0	6.3	4.6	8.2	11.6	<u>98.8</u>	12.1	16.8
	RDI-VT	10.50	5.9	8.9	9.4	13.2	7.4	5.9	9.8	12.3	98.7	14.7	18.6
	RDI-Admix	4.92	6.3	6.5	8.8	12.8	6.0	6.1	10.9	12.2	98.7	13.6	18.2
	RDI-SU	2.36	7.8	11.0	11.4	12.7	9.4	8.2	6.3	8.3	98.7	10.9	18.5
	ODI	6.42	14.3	14.9	16.7	32.3	20.3	13.7	25.3	26.4	95.9	31.6	29.1
	RDI-CFM	2.13	22.9	26.8	26.2	39.1	34.1	27.1	38.6	36.2	95.9	44.8	39.2
	RDI-FTM	2.35	<u>25.8</u>	<u>30.9</u>	<u>32.1</u>	<u>41.7</u>	<u>36.3</u>	<u>30.7</u>	<u>41.4</u>	<u>42.9</u>	94.1	<u>48.1</u>	<u>42.4</u>
	RDI-FTM-E	4.37	34.2	39.3	40.6	54.4	47.0	37.1	51.6	52.4	96.6	59.2	51.2

Table 1. Targeted attack success rates (%) against ten target models. All methods are combined with MI-TI. The best results are shown in bold, and the second best results are underlined. Time (s) denotes the average computation time required to attack a single image.

General settings. We adopt experimental configurations consistent with recent literature [2, 3, 49]. Specifically, we use an ℓ_∞ -norm setting with $\epsilon = 16/255$. We set decay $\mu = 1.0$ and step size $\eta = 2/255$. We perform 300 iterations ($T = 300$) for iterative targeted attacks as per [3]. For optimization of adversarial examples, all methods employ the simple logit loss function [49].

Models. We evaluate our method using 15 pre-trained DNNs, consisting of 10 CNN-based models and 5 transformer-based models. For CNN-based architectures, we employ VGG-16 [35], ResNet-18 (RN-18) [15], ResNet-50 (RN-50) [15], DenseNet-121 (DN-121) [17], Xception (Xcep) [5], MobileNet-v2 (MB-v2) [34], EfficientNet-B0 (EF-B0) [38], Inception ResNet-v2 (IR-v2) [37], Inception-v3 (Inc-v3) [36], and Inception-v4 (Inc-v4) [37]. For Transformer-based architectures, we utilize Vision Transformer (ViT) [11], LeViT [14], ConViT [8], Twins [6], and Pooling-based ViT (PiT) [16].

Baseline attacks. We mainly compare our FTM against ten existing techniques: DI [46], RDI [50], MI [9], TI [10], SI [29], VT [39], Admix [40], ODI [2], SU [43], and CFM [3]. We primarily reference CFM, the current state-of-the-art method for targeted transfer-based attacks that requires no additional training dataset. MI and TI techniques apply across all attack methods, so we omit the ‘MI-TI’ prefix in our references. RDI serves as a common baseline technique in most cases. For DI, RDI, TI, SI, Admix, and ODI, we follow the configurations specified in CFM. For Admix, we also follow CFM to set the mixing weight to $w = 0.2$ and use $N = 3$ mixed images (i.e., $m_2 = 3$

in [40]). Given Admix’s computational intensity, we set the number of scale images in Admix to 1 (i.e., $m_1 = 1$ in [40]) unless otherwise specified. We report the results for ODI instead of RDI-ODI, as ODI performs similarly to RDI-ODI [2, 3]. For SU and CFM, we use the original settings from their papers.

Settings for our FTM. We set the mixing ratio β to 0.01. For FTM-E, we set the number of perturbed models to 2 for all experiments due to the computational cost. Following CFM, we avoid perturbing shallow layers because their low-level features vary significantly with input transforms and may cause excessive disturbance during attacks, as explained in CFM’s paper. Specifically, we perturb layers where the feature map size is smaller than or equal to $\frac{1}{16}$ of the image size. For a pure ViT, we select the outputs of all fully-connected layers. We sample $\alpha_{k,i}$ from $\mathcal{U}(0, 0.75)$, i.e., $\alpha_{max} = 0.75$. We set the probability p to 0.1.

4.2. Experimental Results

Transfer success rates. Table 1 shows the transfer success rates of various attack methods on ten black-box models. When using Inc-v3 as the source model, RDI-FTM-E achieves an average success rate of 51.2%, surpassing the previous best method CFM by 12.0%. The improvement is particularly notable for challenging target models like IR-v2 and Inc-v4, where RDI-FTM-E increases the success rates by 16.2% and 14.4%, respectively. When using RN-50 as the source model, both RDI-FTM and RDI-FTM-E achieve higher success rates than CFM. The results show that the effective feature-level augmentation employed by FTM helps

Source	Attack	Time (s)	ViT	LeViT	ConViT	Twins	PiT	Avg.
RN-50	DI	1.37	0.2	3.5	0.4	1.5	1.7	1.5
	RDI	1.23	0.7	13.2	1.7	6.1	7.0	5.7
	RDI-SI	5.95	2.9	29.4	6.3	15.5	17.9	14.4
	RDI-VT	7.16	2.9	28.1	5.2	15.0	14.0	13.0
	RDI-Admix	3.55	1.3	22.5	2.5	8.5	8.4	8.6
	RDI-SU	2.21	0.8	16.9	2.3	6.9	7.8	6.9
	ODI	4.38	5.1	37.0	10.7	20.1	29.1	20.4
	RDI-CFM	1.39	4.3	46.1	8.9	25.2	24.7	21.8
	RDI-FTM	1.54	<u>5.9</u>	<u>52.9</u>	<u>10.8</u>	<u>32.4</u>	<u>31.5</u>	<u>26.7</u>
	RDI-FTM-E	2.92	6.8	58.6	13.6	35.2	34.9	29.8
Inc-v3	DI	2.01	0.1	0.3	0.0	0.0	0.1	0.1
	RDI	1.76	0.2	1.8	0.2	0.4	0.7	0.7
	RDI-SI	8.11	0.3	4.1	0.9	0.7	3.2	1.8
	RDI-VT	10.5	0.4	5.2	0.8	1.6	1.8	2.0
	RDI-Admix	4.92	0.1	4.1	0.6	1.4	1.4	1.5
	RDI-SU	2.36	0.2	2.0	0.3	1.3	1.0	1.0
	ODI	6.42	0.8	12.4	1.7	3.5	6.7	5.0
	RDI-CFM	2.13	2.1	21.9	3.2	6.1	11.6	8.9
	RDI-FTM	2.35	<u>2.4</u>	<u>25.0</u>	<u>4.5</u>	<u>10.0</u>	<u>15.3</u>	<u>11.5</u>
	RDI-FTM-E	4.37	3.8	32.7	6.8	12.7	20.4	15.3

Table 2. Targeted attack success rates (%) against five transformer-based DNNs. All methods are combined with MI-TI. The best results are shown in bold, and the second best are underlined. Time (s) denotes the average time required to attack a single image.

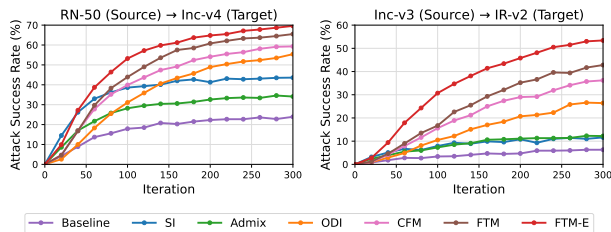


Figure 3. Targeted attack success rates (%) based on the number of iterations. The source model is RN-50 and Inc-v3, respectively.

generate transferable adversarial examples.

Table 2 shows the transfer success rates of various attack methods on five transformer-based models. Our methods also achieve significant improvements over existing methods. For instance, when using RN-50 as the source model, RDI-FTM and RDI-FTM-E improve the targeted attack success rates of CFM by 4.9% and 8.0%, respectively. The results suggest that our method can effectively improve the transferability of adversarial examples across different architectures.

Figure 3 shows the targeted attack success rates based on the number of iterations. We evaluate our methods under different numbers of iterations using two experimental settings: RN-50 \rightarrow Inc-v4 and Inc-v3 \rightarrow IR-v2. The results show that FTM and FTM-E achieve stable performance across different iteration counts. For the RN-50 \rightarrow Inc-v4 setting, SI exhibits superior performance at the beginning of the optimization process. However, as the number of iterations increases, FTM surpasses existing approaches. In the Inc-v3 \rightarrow IR-v2 setting, FTM-E significantly outperforms other methods across the entire range of iterations.

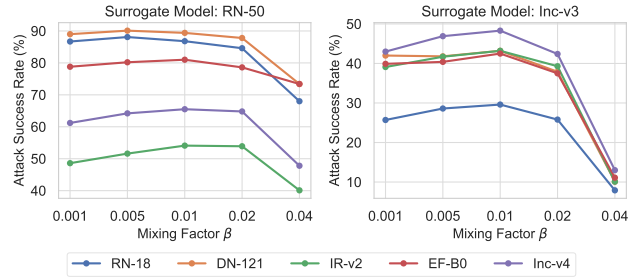


Figure 4. Attack success rates with different mixing ratio β . Each color represents the attack effectiveness on a specific target model.

Computational overhead. We analyze the computational efficiency of different methods and report their costs in Table 2. We use an NVIDIA 3090 GPU to compute the time per image. The results demonstrate that our approach introduces reasonable computational overhead compared to CFM. Specifically, with RN-50 as the source model, RDI-FTM requires an average of 1.54 seconds per image, representing only a 10.8% increase over CFM’s 1.39 seconds. In contrast, alternative methods like SI, VT, and ODI impose substantially higher computational burdens. For instance, VT requires 7.16 seconds per image, and SI requires 5.95 seconds per image. We also include relevant analysis in Figure 1. The result shows that FTM achieves strong attack performance while maintaining low computational cost.

Combination with existing techniques. Table 3 presents transfer success rates of our method combined with ensemble-based method [30], SI, and Admix. Using the ensemble of RN-50 and Inc-v3 as the surrogate model, our RDI-SI-FTM-E achieves 74.5% average success rate, surpassing existing methods. FTM notably enhances performance on transformer-based models. For instance, RDI-SI-FTM achieves 64.3% on PiT, which is 5.0% higher than RDI-SI-CFM (59.3%) with comparable computational cost. These results demonstrate that FTM is a generic technique that combines effectively with existing attack methods.

4.3. Ablation Study

For all ablation experiments, we use RN-50 to generate adversarial examples and evaluate the average success rates on all models from Section 4.1, unless stated otherwise.

Stability with respect to β . Figure 4 shows the transfer success rates of FTM across different mixing ratios β . The success rates on five target models are plotted in distinct colors. When β exceeds 0.04, the success rates decrease substantially across all target models. However, for β values below 0.02, we observe stable attack performance across all models. The results suggest that FTM maintains robust performance within a reasonable range of β values, showing its stability with respect to β .

Compare FTM and CFM using ensemble strategy. Figure 5 shows the attack performance of FTM and CFM

Attack	Time (s)	RN-50 + Inc-v3 \Rightarrow												
		VGG-16	RN-50*	Inc-v3*	DN-121	IR-v2	Inc-v4	Xcep	ViT	LeViT	ConViT	Twins	PiT	Avg.
RDI	3.26	66.9	98.4	98.7	83.1	35.6	42.5	25.4	0.8	22.4	3.2	9.8	10.8	41.5
ODI	7.17	70.9	94.0	96.1	83.4	65.4	69.9	57.6	9.1	52.9	18.6	28.6	42.8	57.4
RDI-CFM	4.39	86.1	<u>98.3</u>	97.0	92.1	71.7	79.9	72.0	10.3	66.5	20.3	41.9	45.8	65.2
RDI-ODI-CFM	7.73	63.9	88.6	81.3	74.1	54.3	56.0	54.3	12.6	49.9	20.9	29.6	41.0	52.2
RDI-Admix-CFM	13.38	86.2	98.1	<u>97.7</u>	92.7	75.1	81.6	76.1	14.0	73.1	24.8	50.7	53.9	68.7
RDI-SI-CFM	22.13	87.5	98.1	97.3	92.7	78.0	81.6	78.0	20.8	76.3	32.9	55.0	59.3	71.5
RDI-FTM	4.47	87.5	97.8	96.7	92.4	75.4	81.7	74.0	14.5	71.0	25.2	49.3	54.4	68.3
RDI-FTM-E	8.81	88.2	98.1	97.1	<u>93.4</u>	76.7	83.4	77.1	18.4	74.9	30.1	53.4	58.0	70.7
RDI-Admix-FTM	14.10	86.0	96.7	96.5	92.2	78.3	83.8	77.3	20.1	75.8	29.9	55.7	58.5	70.9
RDI-SI-FTM	22.66	87.5	96.8	96.2	93.3	<u>79.0</u>	<u>83.6</u>	79.1	<u>25.7</u>	<u>77.7</u>	<u>37.5</u>	<u>59.9</u>	<u>64.3</u>	<u>73.4</u>
RDI-SI-FTM-E	43.43	<u>87.8</u>	97.3	96.7	93.9	79.1	83.5	<u>78.2</u>	27.3	79.2	42.9	62.9	65.6	74.5

Table 3. Targeted attack success rates (%) of combination with different methods. The surrogate model is the ensemble of RN-50 and Inc-v3. All methods are combined with MI-TI. The best results are shown in bold, and the second best are underlined. Time (s) denotes the average time required to attack a single image.

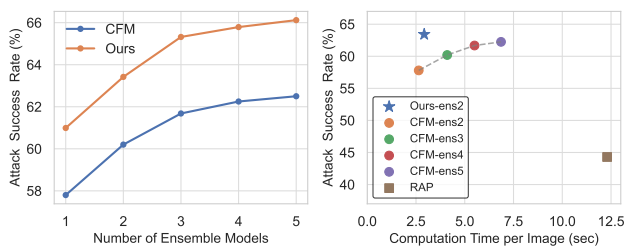


Figure 5. Attack performance and computational costs with different numbers of ensemble models. Left: Our FTM vs. CFM using ensemble strategy. Right: Computational costs of our FTM and RAP. -ens2 means using 2 perturbed models, and so on.

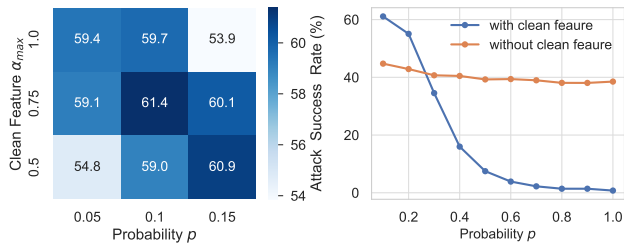


Figure 6. Left: Attack success rates vs. p and α_{max} . Right: Attack success rates vs. p with/without clean features; The blue line is the success rates when the clean features from CFM are integrated with our FTM, while the orange line represents only using our learnable perturbations.

using different numbers of perturbed models. On the left, our FTM consistently outperforms CFM across all ensemble sizes. Notably, FTM with only 2 perturbed models achieves better attack performance than an ensemble of 5 CFM-perturbed models, underscoring FTM’s superior effectiveness. It is also worth mentioning that single FTM and CFM have comparable time complexity (Table 2). On the right, we compare our FTM with RAP [33], and the results show that FTM significantly outperforms RAP in both effectiveness and computational efficiency.

Analysis of probability p and ratio α_{max} . Figure 6 presents an analysis of FTM’s attack success rates under

varying values of p and α_{max} . The left plot shows that FTM achieves optimal performance with $p = 0.1$ and $\alpha_{max} = 0.75$. FTM maintains competitive performance under various parameter configurations, such as $p, \alpha_{max} = 0.15, 0.5$ or $0.05, 1.0$, indicating its parameter stability. The right plot illustrates the impact of clean features on FTM. With clean features enabled, FTM’s performance declines significantly as p increases from 0.1 to 1.0, while FTM without clean features shows stable performance across varying p values. This suggests that although clean features are crucial to FTM’s performance, they also add instability to the attack process. Additionally, setting $p = 1.0$ (where all layers are updated) causes excessive perturbations, making the attack overly aggressive and reducing its effectiveness.

The drop of the blue line in Figure 6 occurs because the clean accuracy of the perturbed surrogate model becomes extremely low (3.8%) at $p = 1.0$ when using clean feature mixup. Without clean feature mixup (orange line), the accuracy remains high at 65.3%. The low accuracy makes it impossible to generate effective adversarial examples, causing the attack success rate of the blue line to drop to near 0.

5. Conclusion

In this work, we study the challenging problem of enhancing transferability in targeted adversarial attacks. Our investigation reveals that feature-level augmentation strategies show promising potential for boosting transferability effectively and efficiently. We introduce Feature Tuning Mixup (FTM), a novel method that incorporates both attack-specific feature perturbations and clean features in the feature space. To optimize the learnable perturbations efficiently, we develop a momentum-based stochastic update strategy. Comprehensive experiments on the ImageNet-compatible dataset demonstrate that FTM achieves substantial improvement over current state-of-the-art methods while maintaining low computational cost.

Acknowledgments. This work was supported in part by HK RGC GRF under Grant PolyU 15201323.

References

- [1] Wieland Brendel, Jonas Rauber, and Matthias Bethge. Decision-based adversarial attacks: Reliable attacks against black-box machine learning models. In *ICLR*, 2018. 2
- [2] Junyoung Byun, Seungju Cho, Myung-Joon Kwon, Hee-Seon Kim, and Changick Kim. Improving the transferability of targeted adversarial examples through object-based diverse input. In *CVPR*, 2022. 1, 3, 5, 6
- [3] Junyoung Byun, Myung-Joon Kwon, Seungju Cho, Yoonji Kim, and Changick Kim. Introducing competition to boost the transferability of targeted adversarial examples through clean feature mixup. In *CVPR*, 2023. 1, 3, 4, 5, 6
- [4] Nicholas Carlini and David Wagner. Towards evaluating the robustness of neural networks. In *IEEE Symposium on Security and Privacy (SP)*, 2017. 2
- [5] Francois Chollet. Xception: Deep learning with depthwise separable convolutions. In *CVPR*, 2017. 6
- [6] Xiangxiang Chu, Zhi Tian, Yuqing Wang, Bo Zhang, Haibing Ren, Xiaolin Wei, Huaxia Xia, and Chunhua Shen. Twins: Revisiting the design of spatial attention in vision transformers. In *NeurIPS*, 2021. 6
- [7] Xuelong Dai, Kaisheng Liang, and Bin Xiao. Advdiff: Generating unrestricted adversarial examples using diffusion models. In *ECCV*, 2024. 2
- [8] Stéphane d’Ascoli, Hugo Touvron, Matthew L. Leavitt, Ari S. Morcos, Giulio Biroli, and Levent Sagun. Convit: Improving vision transformers with soft convolutional inductive biases. In *ICML*, 2021. 6
- [9] Yinpeng Dong, Fangzhou Liao, Tianyu Pang, Hang Su, Jun Zhu, Xiaolin Hu, and Jianguo Li. Boosting adversarial attacks with momentum. In *CVPR*, 2018. 1, 2, 3, 4, 6
- [10] Yinpeng Dong, Tianyu Pang, Hang Su, and Jun Zhu. Evading defenses to transferable adversarial examples by translation-invariant attacks. In *CVPR*, 2019. 1, 3, 6
- [11] Alexey Dosovitskiy, Lucas Beyer, Alexander Kolesnikov, Dirk Weissenborn, Xiaohua Zhai, Thomas Unterthiner, Mostafa Dehghani, Matthias Minderer, Georg Heigold, Sylvain Gelly, Jakob Szehkoreit, and Neil Houlsby. An image is worth 16x16 words: Transformers for image recognition at scale. *ICLR*, 2021. 6
- [12] Kevin Eykholt, Ivan Evtimov, Earlene Fernandes, Bo Li, Amir Rahmati, Chaowei Xiao, Atul Prakash, Tadayoshi Kohno, and Dawn Song. Robust physical-world attacks on deep learning visual classification. In *CVPR*, 2018. 2
- [13] Ian J. Goodfellow, Jonathon Shlens, and Christian Szegedy. Explaining and harnessing adversarial examples. In *ICLR*, 2015. 1, 2
- [14] Benjamin Graham, Alaaeldin El-Nouby, Hugo Touvron, Pierre Stock, Armand Joulin, Hervé Jégou, and Matthijs Douze. Levit: a vision transformer in convnet’s clothing for faster inference. In *ICCV*, 2021. 6
- [15] Kaiming He, Xiangyu Zhang, Shaoqing Ren, and Jian Sun. Deep residual learning for image recognition. In *CVPR*, 2016. 6
- [16] Byeongho Heo, Sangdoon Yun, Dongyoon Han, Sanghyuk Chun, Junsuk Choe, and Seong Joon Oh. Rethinking spatial dimensions of vision transformers. In *ICCV*, 2021. 6
- [17] Gao Huang, Zhuang Liu, Laurens Van Der Maaten, and Kilian Q Weinberger. Densely connected convolutional networks. In *CVPR*, 2017. 6
- [18] Qian Huang, Isay Katsman, Zeqi Gu, Horace He, Serge J. Belongie, and Ser-Nam Lim. Enhancing adversarial example transferability with an intermediate level attack. In *ICCV*, 2019. 3
- [19] Andrew Ilyas, Shibani Santurkar, Dimitris Tsipras, Logan Engstrom, Brandon Tran, and Aleksander Madry. Adversarial examples are not bugs, they are features. In *NeurIPS*, 2019. 2
- [20] Nathan Inkawhich, Wei Wen, Hai (Helen) Li, and Yiran Chen. Feature space perturbations yield more transferable adversarial examples. In *CVPR*, 2019. 3
- [21] Nathan Inkawhich, Kevin J. Liang, Lawrence Carin, and Yiran Chen. Transferable perturbations of deep feature distributions. In *ICLR*, 2020. 3
- [22] Nathan Inkawhich, Kevin J. Liang, Binghui Wang, Matthew Inkawhich, Lawrence Carin, and Yiran Chen. Perturbing across the feature hierarchy to improve standard and strict blackbox attack transferability. In *NeurIPS*, 2020. 3
- [23] Alexey Kurakin, Ian J. Goodfellow, and Samy Bengio. Adversarial examples in the physical world. In *ICLR (Workshop)*, 2017. 1, 3
- [24] Maosen Li, Cheng Deng, Tengjiao Li, Junchi Yan, Xinbo Gao, and Heng Huang. Towards transferable targeted attack. In *CVPR*, 2020. 3
- [25] Qizhang Li, Yiwen Guo, and Hao Chen. Yet another intermediate-level attack. In *ECCV*, 2020. 3
- [26] Yanjie Li, Yiquan Li, Xuelong Dai, Songtao Guo, and Bin Xiao. Physical-world optical adversarial attacks on 3d face recognition. In *CVPR*, 2023. 2
- [27] Yanjie Li, Kaisheng Liang, and Bin Xiao. UV-attack: Physical-world adversarial attacks on person detection via dynamic-NeRF-based UV mapping. In *ICLR*, 2025. 2
- [28] Kaisheng Liang and Bin Xiao. Styleless: Boosting the transferability of adversarial examples. In *CVPR*, 2023. 2
- [29] Jiadong Lin, Chuanbiao Song, Kun He, Liwei Wang, and John E. Hopcroft. Nesterov accelerated gradient and scale invariance for adversarial attacks. In *ICLR*, 2020. 1, 3, 6
- [30] Yanpei Liu, Xinyun Chen, Chang Liu, and Dawn Song. Delving into transferable adversarial examples and black-box attacks. In *ICLR*, 2017. 3, 7
- [31] Aleksander Madry, Aleksandar Makelov, Ludwig Schmidt, Dimitris Tsipras, and Adrian Vladu. Towards deep learning models resistant to adversarial attacks. In *ICLR*, 2018. 1, 2, 5
- [32] Muzammal Naseer, Salman Khan, Munawar Hayat, Fahad Shahbaz Khan, and Fatih Porikli. On generating transferable targeted perturbations. In *ICCV*, 2021. 3
- [33] Zeyu Qin, Yanbo Fan, Yi Liu, Li Shen, Yong Zhang, Jue Wang, and Baoyuan Wu. Boosting the transferability of adversarial attacks with reverse adversarial perturbation. In *NeurIPS*, 2022. 3, 8
- [34] Mark Sandler, Andrew Howard, Menglong Zhu, Andrey Zhmoginov, and Liang-Chieh Chen. Mobilenetv2: Inverted residuals and linear bottlenecks. In *CVPR*, 2018. 6

- [35] Karen Simonyan and Andrew Zisserman. Very deep convolutional networks for large-scale image recognition. In *ICLR*, 2015. 6
- [36] Christian Szegedy, Vincent Vanhoucke, Sergey Ioffe, Jonathon Shlens, and Zbigniew Wojna. Rethinking the inception architecture for computer vision. In *CVPR*, 2016. 6
- [37] Christian Szegedy, Sergey Ioffe, Vincent Vanhoucke, and Alexander A. Alemi. Inception-v4, inception-resnet and the impact of residual connections on learning. In *AAAI*, 2017. 6
- [38] Mingxing Tan and Quoc V. Le. Efficientnet: Rethinking model scaling for convolutional neural networks. In *ICML*, 2019. 6
- [39] Xiaosen Wang and Kun He. Enhancing the transferability of adversarial attacks through variance tuning. In *CVPR*, 2021. 1, 3, 6
- [40] Xiaosen Wang, Xuanran He, Jingdong Wang, and Kun He. Admix: Enhancing the transferability of adversarial attacks. In *ICCV*, 2021. 1, 3, 6
- [41] Zhibo Wang, Hengchang Guo, Zhifei Zhang, Wenxin Liu, Zhan Qin, and Kui Ren. Feature importance-aware transferable adversarial attacks. In *ICCV*, 2021. 3
- [42] Zhibo Wang, Hongshan Yang, Yunhe Feng, Peng Sun, Hengchang Guo, Zhifei Zhang, and Kui Ren. Towards transferable targeted adversarial examples. In *CVPR*, 2023. 3
- [43] Zhipeng Wei, Jingjing Chen, Zuxuan Wu, and Yu-Gang Jiang. Enhancing the self-universality for transferable targeted attacks. In *CVPR*, 2023. 1, 3, 5, 6
- [44] Dongxian Wu, Yisen Wang, Shu-Tao Xia, James Bailey, and Xingjun Ma. Skip connections matter: On the transferability of adversarial examples generated with resnets. In *ICLR*, 2020. 3
- [45] Weibin Wu, Yuxin Su, Michael R Lyu, and Irwin King. Improving the transferability of adversarial samples with adversarial transformations. In *CVPR*, 2021. 3
- [46] Cihang Xie, Zhishuai Zhang, Yuyin Zhou, Song Bai, Jianyu Wang, Zhou Ren, and Alan L. Yuille. Improving transferability of adversarial examples with input diversity. In *CVPR*, 2019. 1, 3, 6
- [47] Xiao Yang, Yinpeng Dong, Tianyu Pang, Hang Su, and Jun Zhu. Boosting transferability of targeted adversarial examples via hierarchical generative networks. In *ECCV*, 2022. 3
- [48] Jianping Zhang, Weibin Wu, Jen-tse Huang, Yizhan Huang, Wenxuan Wang, Yuxin Su, and Michael R Lyu. Improving adversarial transferability via neuron attribution-based attacks. In *CVPR*, 2022. 3
- [49] Zhengyu Zhao, Zhuoran Liu, and Martha Larson. On success and simplicity: A second look at transferable targeted attacks. In *NeurIPS*, 2021. 1, 3, 5, 6
- [50] Junhua Zou, Zhisong Pan, Junyang Qiu, Xin Liu, Ting Rui, and Wei Li. Improving the transferability of adversarial examples with resized-diverse-inputs, diversity-ensemble and region fitting. In *ECCV*, 2020. 3, 6

Supplementary Material for Improving Transferable Targeted Attacks with Feature Tuning Mixup

In the supplementary material, we provide additional experimental results on parameter p in Chapter A.1. Then, in Chapters A.2, A.3, and A.4, we present additional results demonstrating the effectiveness and efficiency of FTM across different surrogate and targeted models. Finally, Chapter A.5 includes visualizations of adversarial examples generated by our FTM.

A. Additional Experiments

A.1. Supplementary results on the analysis of p

We have shown in Section 4.3 (Ablation Study) that the attack success rate when using clean feature mixup drops to near 0 in Figure 6 due to the low clean accuracy of the perturbed surrogate model. Table 4 shows the clean accuracy of the perturbed surrogate model with varying values of p . The results demonstrate that increasing p leads to extremely low clean accuracy when using clean feature mixup in FTM, which explains the rapid decline of the blue line in Figure 6. In contrast, without clean feature mixup, the clean accuracy remains stable, maintaining 65.3% even at $p = 1.0$. Consequently, the corresponding orange line in Figure 6 exhibits relatively stable behavior. Notably, as shown in the left plot of Figure 6 our FTM performs stably around the optimal hyperparameter p and α_{max} .

Ablation	Parameter p									
	0.1	0.2	0.3	0.4	0.5	0.6	0.7	0.8	0.9	1.0
w/ clean feature mixup	51.9	28.3	14.0	10.8	8.2	6.0	5.4	4.9	4.3	3.8
w/o clean feature mixup	79.8	73.3	69.7	68.6	67.0	66.4	66.0	65.8	65.4	65.3

Table 4. Accuracy (%) of clean images on the perturbed surrogate model with varying parameter p .

A.2. Attacking black-box multimodal LLMs

FTM can be used to attack multimodal LLMs. We use four commercial LLMs for evaluation, including Qwen2-VL, Llama-3.2, Claude-3.5, and GPT-4o. We randomly select 100 images from the ImageNet-compatible dataset and generate targeted adversarial examples on ViT using RDI-FTM-E. For each generated targeted adversarial example, we use the prompt “Is this image a photo of {target label}? Yes or No?” to obtain the predictions of the LLMs. Table 5 shows that our method achieves an average attack success rate of 40.5%.

Response	Qwen2-VL	Llama-3.2	Claude-3.5	GPT-4o	Avg
Total	100	100	100	100	100 %
Refuse to Answer	0	10	0	0	2.50 %
Uncertain	1	5	1	0	1.75 %
Attack Failed	52	42	54	73	55.25 %
Attack Succeeded	47	43	45	27	40.50 %

Table 5. Evaluation on multimodal LLMs. The targeted adversarial examples are generated on ViT using RDI-FTM-E.

A.3. Evaluation with different surrogate models

We report the targeted attack success rates when using DN-121 or LeViT as the surrogate model in Table 6. The results demonstrate that, across all black-box attack scenarios, our methods consistently outperform existing approaches, regardless of whether DN-121 or LeViT is used as the surrogate model.

We report the targeted attack success rates using ensemble-based surrogate models in Table 7. We use two settings for the ensemble-based surrogate models: RN-50 + Inc-v3 and RN-50 + LeViT. The results show that our methods can be combined with current ensemble-based methods to further improve the attack success rates.

A.4. Efficiency of FTM on attacking ViT

We show that FTM remains effective and efficient when using ViT as the surrogate model. Unlike other models in Section 4.1, ViT’s feature map size does not decrease with depth. As analyzed in Section 3.3, FTM is theoretically efficient and adaptable to various architectures, including ViT. Tables 8 and 9 confirm that FTM maintains low computational complexity when using ViT as the surrogate model. Our RDI-FTM-E-SI $_{m_1=2}$ generates adversarial examples in just 3.82 seconds on average while significantly outperforming existing attacks. In RDI-FTM-E-SI $_{m_1=2}$, the two copies of the surrogate model in FTM-E use scaled inputs (1 and 0.5, respectively), preserving efficiency. The parameter m_1 in RDI-FTM-E-SI $_{m_1=2}$ is set to 2 to correspond with the two copies of the surrogate model used in FTM-E. Overall, our results validate FTM’s effectiveness and efficiency across different architectures.

A.5. Visualization of targeted adversarial examples

Figure 7 and Figure 8 present visualizations of adversarial examples crafted by different targeted transfer-based attack methods.

Attack	DN-121 \Rightarrow											
	VGG-16	RN-50	Inc-v3	DN-121*	IR-v2	Inc-v4	Xcep	ViT	LeViT	ConViT	Twins	PiT
DI	37.1	44.4	7.1	98.7	4.3	8.3	5.2	0.2	3.0	0.4	1.0	1.1
RDI	42.1	55.7	20.8	98.5	12.8	18.8	10.1	0.8	8.5	1.3	3.7	4.5
RDI-Admix	53.2	67.6	31.1	98.3	20.1	26.5	17.8	1.0	14.7	1.7	6.8	7.4
RDI-Admix ₅	49.6	65.3	41.0	<u>98.6</u>	28.9	34.3	21.6	2.4	21.8	3.4	10.5	14.2
RDI-SI	45.4	60.1	34.3	<u>98.6</u>	22.0	25.8	16.1	2.0	16.1	2.4	8.2	11.7
RDI-VT	47.7	62.1	31.5	<u>98.6</u>	25.4	27.2	20.3	2.2	19.2	3.5	8.3	11.7
RDI-ODI	64.2	71.7	52.8	98.0	39.8	45.9	31.4	3.3	26.9	7.4	14.7	21.9
RDI-CFM	76.2	83.9	56.1	97.8	43.6	53.8	41.1	3.6	32.8	6.4	17.3	21.1
RDI-FTM	<u>77.3</u>	<u>85.6</u>	<u>62.8</u>	98.2	<u>46.9</u>	<u>58.4</u>	<u>46.0</u>	<u>3.7</u>	<u>40.0</u>	<u>8.2</u>	<u>21.6</u>	<u>26.5</u>
RDI-FTM-E	79.5	87.6	64.6	98.0	48.7	60.1	47.6	4.2	43.4	8.9	24.4	26.7

Attack	LeViT \Rightarrow											
	VGG-16	RN-50	Inc-v3	DN-121	IR-v2	Inc-v4	Xcep	ViT	LeViT*	ConViT	Twins	PiT
DI	1.6	2.5	4.2	2.7	1.8	2.6	2.3	0.6	100	4.2	9.3	10.3
RDI	3.0	3.5	5.4	4.1	3.6	4.6	2.3	1.1	100	7.9	13.8	22.1
RDI-Admix	6.5	8.3	9.9	8.8	5.8	7.2	5.5	3.3	100	10.7	23.3	30.9
RDI-Admix ₅	5.3	8.1	13.9	12.4	9.9	8.4	7.2	8.0	99.9	20.6	30.0	47.2
RDI-SI	3.4	6.3	10.6	10.0	6.4	5.4	5.1	4.3	100	18.1	24.1	38.4
RDI-VT	5.3	7.2	12.0	10.1	8.3	8.8	8.9	6.3	99.9	18.7	27.2	40.5
RDI-ODI	21.0	25.0	40.9	38.3	25.7	31.2	26.3	15.3	98.7	34.1	43.8	66.1
RDI-CFM	27.3	30.3	39.8	39.0	23.6	30.1	27.2	18.4	100	45.5	63.8	75.7
RDI-FTM	<u>41.3</u>	<u>41.9</u>	<u>56.9</u>	<u>54.2</u>	<u>39.8</u>	<u>46.5</u>	<u>42.2</u>	<u>31.1</u>	99.9	<u>63.2</u>	<u>77.5</u>	<u>86.7</u>
RDI-FTM-E	50.1	52.4	62.8	63.1	48.4	53.2	49.2	40.3	99.9	72.2	86.2	93.0

Table 6. Targeted attack success rates (%) using DN-121 or LeViT as surrogate model. All methods are combined with MI-TI. The best results are shown in bold, and the second best results are underlined. The surrogate models are marked with * in the first column.

Attack	RN-50 + Inc-v3 \Rightarrow											
	VGG-16	RN-50*	Inc-v3*	DN-121	IR-v2	Inc-v4	Xcep	ViT	LeViT	ConViT	Twins	PiT
DI	63.5	99.0	99.2	77.0	16.6	24.0	12.5	0.2	7.3	0.7	3.1	2.6
RDI	66.9	<u>98.4</u>	98.7	83.1	35.6	42.5	25.4	0.8	22.4	3.2	9.8	10.8
RDI-SI	70.1	98.0	98.9	89.3	53.3	57.3	40.0	4.5	40.7	8.8	21.4	27.4
RDI-VT	66.4	<u>98.4</u>	98.8	83.1	51.6	56.6	40.7	5.0	39.6	8.4	21.6	22.7
RDI-Admix	72.9	<u>98.4</u>	<u>99.1</u>	88.0	46.3	58.3	36.5	1.8	33.4	4.5	15.4	17.1
RDI-ODI	70.9	94.0	96.1	83.4	65.4	69.9	57.6	9.1	52.9	18.6	28.6	42.8
RDI-CFM	86.1	98.3	97.0	92.1	71.7	79.9	72.0	10.3	66.5	20.3	41.9	45.8
RDI-FTM	<u>87.5</u>	97.8	96.7	<u>92.4</u>	<u>75.4</u>	<u>81.7</u>	<u>74.0</u>	<u>14.5</u>	<u>71.0</u>	<u>25.2</u>	<u>49.3</u>	<u>54.4</u>
RDI-FTM-E	88.2	98.1	97.1	93.4	76.7	83.4	77.1	18.4	74.9	30.1	53.4	58.0

Attack	RN-50 + LeViT \Rightarrow											
	VGG-16	RN-50*	Inc-v3	DN-121	IR-v2	Inc-v4	Xcep	ViT	LeViT*	ConViT	Twins	PiT
DI	71.3	99.2	29.5	80.3	16.2	23.7	15.4	1.2	100	6.7	18.2	20.8
RDI	75.3	98.7	55.7	87.8	35.1	41.9	29.6	4.2	99.4	14.6	34.3	41.1
RDI-SI	78.1	<u>98.9</u>	74.0	92.8	53.1	57.4	45.5	10.6	<u>99.9</u>	30.5	52.2	67.1
RDI-VT	77.4	<u>98.9</u>	66.4	88.1	50.7	56.0	48.4	14.6	99.1	30.3	53.9	60.7
RDI-Admix	82.3	98.8	64.8	91.2	43.6	53.9	41.0	7.6	<u>99.9</u>	17.4	43.9	48.8
RDI-ODI	81.9	96.6	81.6	89.6	69.9	73.4	67.9	27.8	97.4	52.7	66.5	81.0
RDI-CFM	88.5	98.8	84.1	92.1	69.5	78.7	72.1	26.4	99.8	51.6	77.5	81.3
RDI-FTM	<u>89.2</u>	98.4	<u>86.4</u>	<u>93.0</u>	<u>74.2</u>	<u>81.0</u>	<u>77.1</u>	<u>41.0</u>	99.5	<u>66.1</u>	<u>85.5</u>	<u>89.2</u>
RDI-FTM-E	90.0	98.1	86.7	93.9	76.7	82.4	80.1	51.5	99.7	72.6	87.9	90.8

Table 7. Targeted attack success rates (%) using ensemble-based surrogate models. All methods are combined with MI-TI. The best results are shown in bold, and the second best results are underlined. The surrogate models are marked with * in the first column.

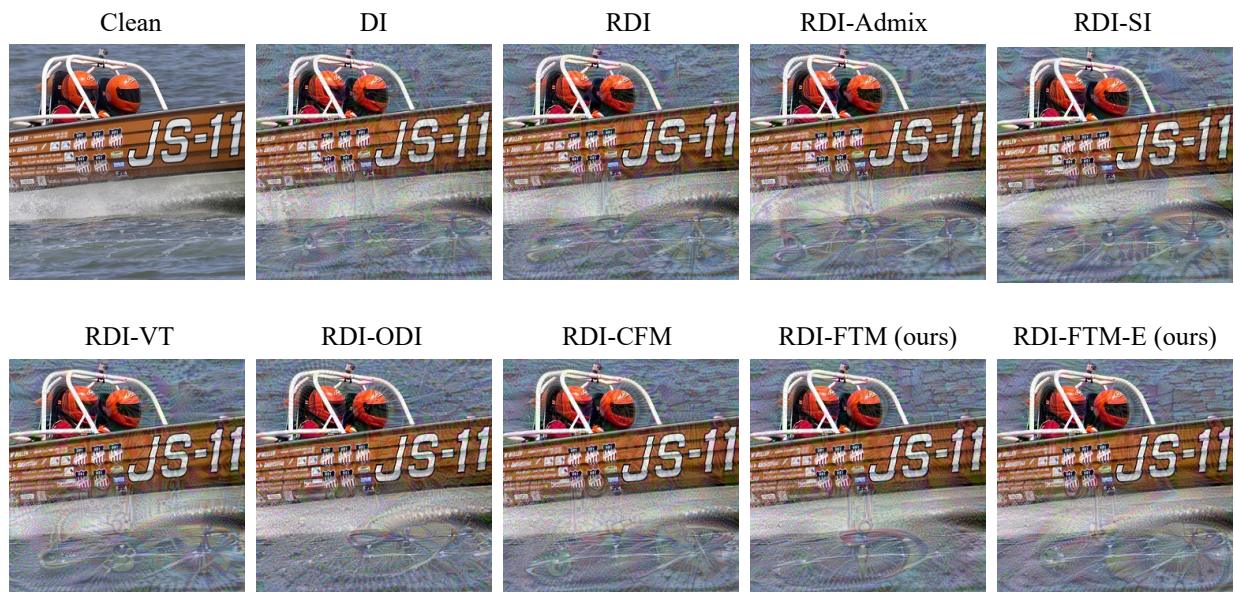
Source	Attack	Time (s)	VGG-16	RN-18	RN-50	DN-121	Xcep	MB-v2	EF-B0	IR-v2	Inc-v3	Inc-v4	Avg.
ViT	RDI	1.76	2.4	2.4	3.1	5.2	3.5	3.6	10.6	4.4	5.3	4.3	4.5
	RDI-VT	10.20	2.5	3.6	4.1	7.1	5.9	4.1	13.4	7.4	5.5	5.4	5.9
	RDI-Admix	5.11	5.4	5.4	6.9	11.5	6.7	6.9	18.7	8.1	10.1	8.0	8.8
	RDI-SI	8.38	4.2	8.2	9.5	17.6	10.2	9.1	24.7	13.3	18.0	12.1	12.7
	RDI-ODI	4.53	10.2	12.7	14.3	22.1	18.6	12.1	32.2	<u>22.5</u>	22.3	20.7	18.8
	RDI-CFM	1.80	10.8	14.2	14.9	21.0	14.9	15.0	31.9	15.0	18.9	17.1	17.4
	RDI-FTM	1.92	11.6	15.1	14.6	22.1	16.7	18.6	31.8	15.8	20.5	18.0	18.5
	RDI-FTM-E	3.81	<u>13.4</u>	<u>18.1</u>	<u>18.3</u>	<u>26.5</u>	<u>19.6</u>	<u>19.5</u>	<u>37.2</u>	19.8	<u>23.0</u>	<u>21.3</u>	<u>21.7</u>
	RDI-FTM-E-SI _{m₁=2}	3.82	24.0	29.1	30.0	41.5	28.9	31.3	54.7	30.9	39.3	31.8	34.2

Table 8. Targeted attack success rates (%) against ten target models, with ViT as the surrogate model. All methods are combined with MI-TI. The best results are shown in bold, and the second best results are underlined. Time (s) denotes the average computation time required to attack a single image. RDI-FTM-E-SI_{m₁=2} denotes using scaled input for RDI-FTM-E.

Source	Attack	Time (s)	ViT	LeViT	ConViT	Twins	PiT	Avg.
ViT	RDI	1.76	99.5	24.3	23.3	11.7	26.0	37.0
	RDI-VT	10.20	98.3	32.0	29.7	15.3	35.7	42.2
	RDI-Admix	5.11	<u>99.1</u>	39.0	34.6	18.5	40.5	46.3
	RDI-SI	8.38	98.4	<u>58.4</u>	<u>69.2</u>	<u>38.8</u>	<u>63.8</u>	<u>65.7</u>
	RDI-ODI	4.53	87.6	45.9	42.1	29.5	49.3	50.9
	RDI-CFM	1.80	96.5	47.2	50.1	27.4	48.8	54.0
	RDI-FTM	1.92	94.3	50.5	53.3	31.0	52.6	56.3
	RDI-FTM-E	3.81	96.0	54.9	55.6	36.3	55.8	59.7
	RDI-FTM-E-SI _{m₁=2}	3.82	96.3	71.2	74.8	54.7	74.6	74.3

Table 9. Targeted attack success rates (%) against five transformer-based DNNs, with ViT as the surrogate model. All methods are combined with MI-TI. The best results are shown in bold, and the second best are underlined. Time (s) denotes the average time required to attack a single image. RDI-FTM-E-SI_{m₁=2} denotes using scaled input for RDI-FTM-E.

True Label: speedboat
Target Label: unicycle, monocycle



True Label: soccer ball
Target Label: potter's wheel

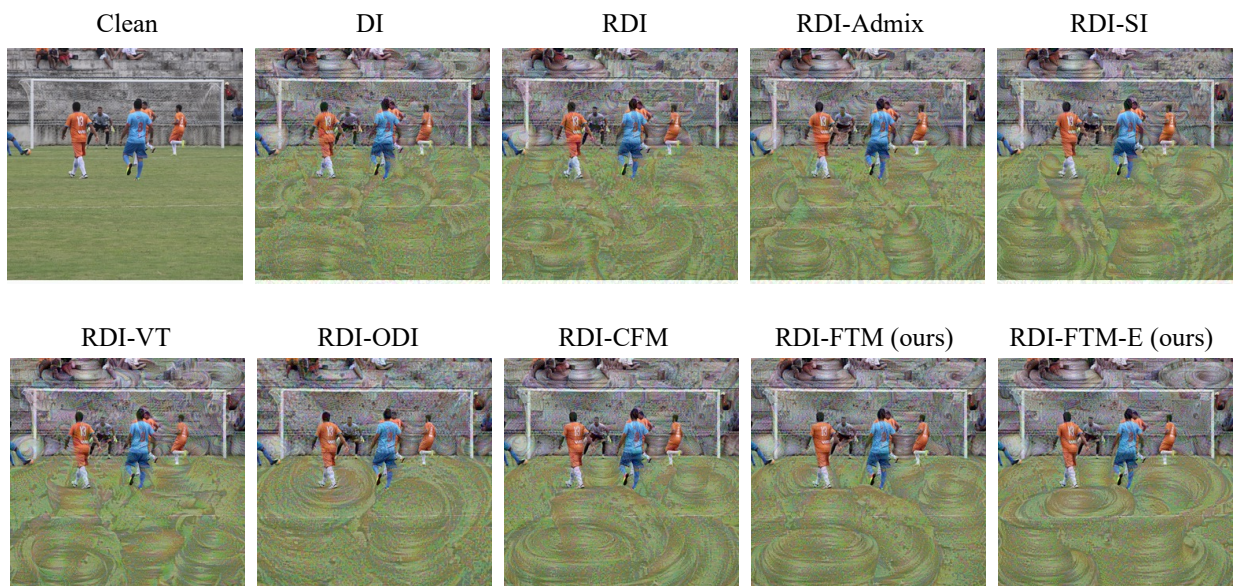
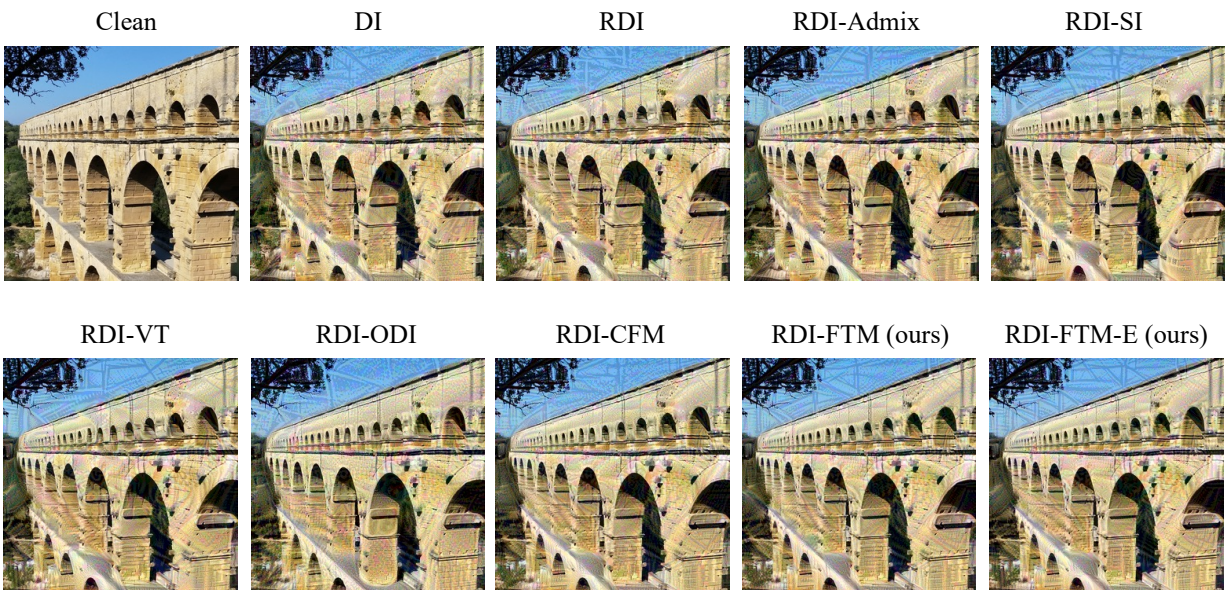


Figure 7. Visualization of targeted adversarial examples generated by different attack methods. The surrogate model used for attack generation is an ensemble of RN-50 and Inc-v3.

True Label: viaduct
Target Label: bullet train



True Label: lakeside, lakeshore
Target Label: dhole, Cuon alpinus

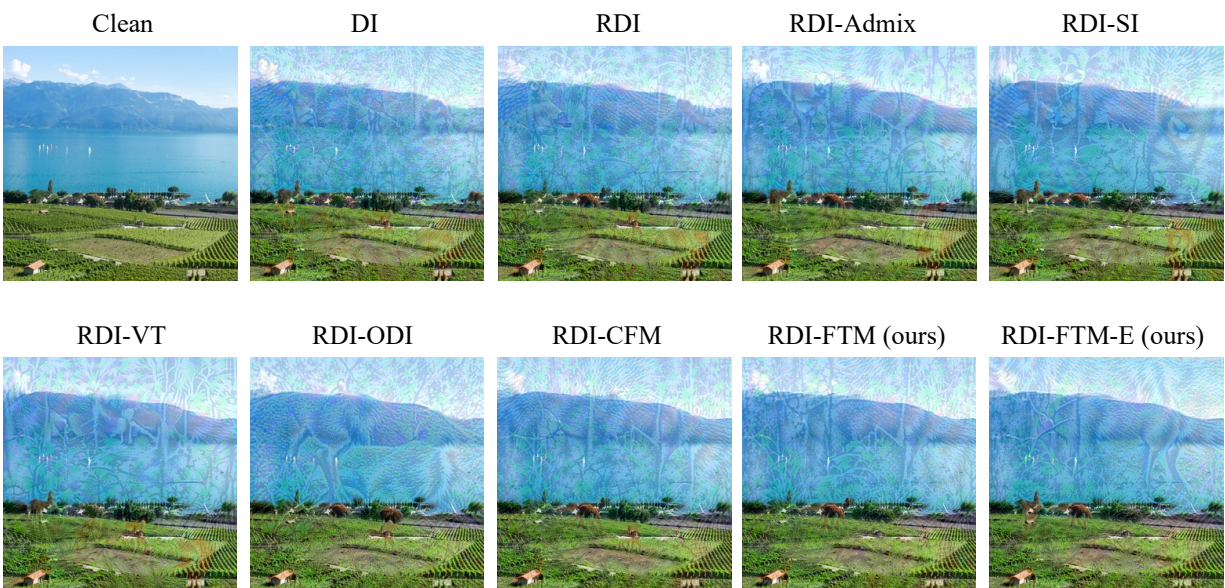


Figure 8. Visualization of targeted adversarial examples generated by different attack methods. The surrogate model used for attack generation is an ensemble of RN-50 and LeViT.